Dalton Transactions

PAPER

View Article Online
View Journal | View Issue

Functionalized mesoporous solids based on magadiite and [Al]-magadiite†

Cite this: *Dalton Trans.*, 2014, **43**, 10471

Hipassia M. Moura and Heloise O. Pastore*

Received 19th December 2013,
Accepted 20th February 2014

DOI: 10.1039/c3dt53571a

www.rsc.org/dalton

Novel hybrid mesoporous and functionalized materials with controllable surface area and pore dimensions with functional basic sites ($-NH_2$) were synthesized from magadiite and [Al]-magadiite as layered silicate precursors. The variable pore structure and properties of these materials were investigated in these solids by using different CTA^+/Na^+ (CTA^+ = cetyltrimethylammonium cation) molar ratios in the pre-modification step with aminopropyltriethoxysilane (APTS) and tetraethoxysilane (TEOS). Characterizations were carried out by different techniques to probe the effects of the amounts of interlayer surfactant in the synthesis of the pillared and/or grafted materials. The crystalline structures of magadiite and [Al]-magadiite layers were maintained as evidenced by FT-IR and SAED and contain pillars and aminopropyl groups in the interlayer space. The hybrid solids were compared to the pillared forms (H. M. Moura, F. A. Bonk and H. O. Pastore, *Eur. J. Mineral.*, 2012, **24**, 903) and to the aminopropyl-grafted forms and presented the properties of both solids with the CO_2 adsorption capability improved considerably.

1. Introduction

Pillared materials with large surface areas and pore volumes are interesting substrates for many applications in the field of adsorption and catalysis. Pillared clays show a characteristic porous structure, mainly driven by the number and size of the pillars in the interlayer region, which are, in turn, influenced by the cation exchange capacity of the original clay mineral, among other factors.[1]

The preparation of these pillared solids involves the polymerization of silica sources directed by a template of surfactants into the interlayer gallery of the clay, to afford materials with surface areas reaching values up to 1000 $m^2 g^{-1}$.[2–6] Often, tetraethoxysilane is the silica source, although other silanes, such as phenyl or methyltriethoxysilane, may be used.[6,7] The surface properties of these materials can be changed by post-synthesis methods using the reactive silanol groups on the surface. The pre-intercalation of cetyltrimethylammonium cations (CTA^+) at different concentrations and subsequent pillaring by TEOS hydrolysis into magadiite interlayer were investigated before.[8] The process resulted in a mesoporous pillared clay with significant variations in surface areas and pore sizes and with the pore size controlled by the molar ratio between the sodium counter-ion present in lamellar silicates (Na^+/CTA^+) and the surfactant to be inserted; it is not dependent solely on the molecular length of surfactant.

The development of inorganic hybrid nanocomposites by alkoxysilylation with 4,4′-biphenyl-bridged alkoxysilane compounds in ilerite has already been described.[9] A porous benzene–silica hybrid clay heterostructure, prepared by condensation of bis(triethoxysilyl)benzene and tetraethylorthosilicate (TEOS), has been used to prepare solids for adsorbing volatile organic compounds.[10,11] Among possible functions, the adsorptive properties of organically modified layered solids have been investigated extensively. Ogawa's group has reported the preparation of organosilylated layered silicates with controlled microstructures and properties toward selective adsorbents.[12,13] For example, the inorganic–organic hybrid hosts bind *n*-alkyl alcohols in their expandable interlayer spaces with the cooperative effects of the organophilic octyl groups and possible hydrogen bonding. The octylsilylated magadiites adsorb *n*-alkyl alcohols quantitatively to give composites with layered hybrids with the controlled gallery heights.[14,15]

Also, the grafting of amine groups on the surface of mesoporous silica has been reported for modifying the hydrophobic properties of the resulting material;[16] the improvement in adsorption of carbon dioxide has been the subject of recent studies.[17–19]

In this sense, we report here the synthesis of aminopropyl-functionalized mesoporous heterostructures in a single step based on magadiite and [Al]-magadiite silicate with designed pore structure, accessibility and activity, using various CTA^+ concentrations during the synthesis. The presence of

Institute of Chemistry, University of Campinas, Monteiro Lobato St 270, CEP 13083 861, Campinas/São Paulo, Brazil. E-mail: gpmmm@iqm.unicamp.br; Tel: +55 19 3521 3017

†Electronic supplementary information (ESI) available. See DOI: 10.1039/c3dt53571a

aluminum in the framework of these pillared heterostructures can also afford interesting catalysts.

2. Experimental

2.1. Magadiite and [Al]-magadiite

These solids were synthesized as described before by Moura *et al.*[20] The Si/Al ratio in the final solid was determined by ICP to be 13.6 and the Si/Al ratio on the surface is 1.0 as determined by electron spectroscopy for chemical analysis.

2.2. Cetyltrimethylammonium-magadiites

The ion exchange was performed by suspending 1.0 g of magadiite/[Al]-magadiite in 1 L of MiliQ water. Considering the general formula of magadiite as $Na_2Si_{14}O_{29}{\cdot}8H_2O$, CTA^+ exchange was performed at CTA/Na molar percentages equal to 25, 50, 75 and 100. After that, cetyltrimethylammonium bromide was added and the mixture was kept under magnetic stirring for 4 h. Finally, the material was washed until the end of foaming and dried in air at room temperature. The samples were named CTA-magaX/CTA-[Al]-magaX (where X corresponds to the real CTA/Na molar percentage confirmed by carbon, hydrogen and nitrogen elemental analyses, CHN).

2.3. Synthesis of the hybrid materials

A solution of pre-hydrolyzed TEOS in ethanol was added to the CTA^+-magadiite suspensions (1 wt%) as reported for pillared materials.[2] After 2 h of reaction, a solution of pre-hydrolyzed APTS in ethanol (for 1 h) was added to the mixture and maintained under stirring for another hour. The mixture was transferred to a stainless steel autoclave lined with Teflon for the hydrothermal treatment for 66 h at 100 °C. The TEOS : APTS molar ratio was equal to 1. The solids were washed, dried and named HYB-magaX and HYB-[Al]-magaX for materials derived from magadiite and [Al]-magadiite, respectively, and X corresponds to the CTA/Na molar percentage on the starting magadiite.

Pillarization and grafting processes were performed according to Zhu *et al.*[21] and Wang *et al.*,[22] respectively, and are detailed in the ESI.†

2.4. Characterization

Confirmation of the formation of desired materials was made by X-ray diffraction (XRD), transmission electron microscopy with selected area electron diffraction (TEM-SAED), field emission scanning electron microscopy (FE SEM), elemental analyses of carbon, hydrogen, nitrogen, sodium and aluminum, Fourier-transform infrared spectroscopy (FTIR), solid-state nuclear magnetic resonance and porosity measurements. The details are described in the ESI.†

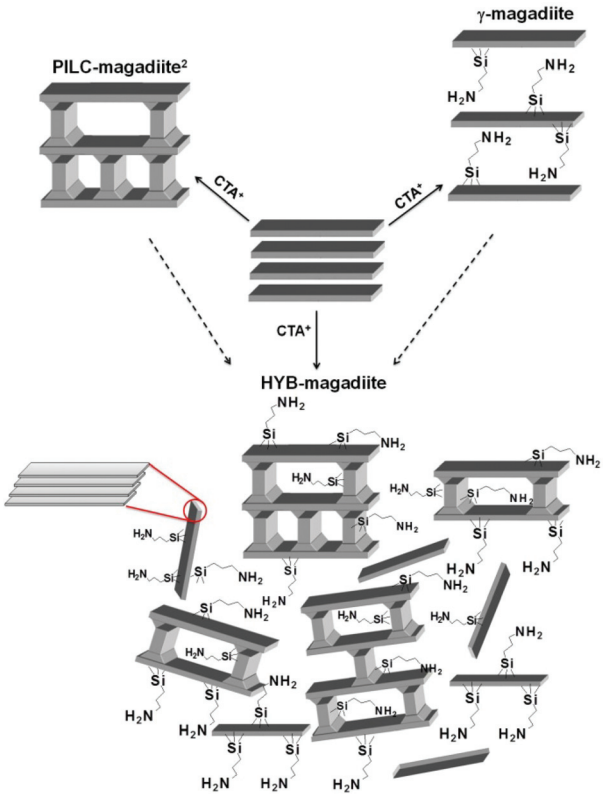

Scheme 1 Pictorial representation of magadiite as a precursor to pillared, grafted and functionalized mesoporous heterostructures (PILC-, γ- and HYB-magadiites, respectively).

3. Results and discussion

To obtain solids with grafted functional groups and with designed porosity from lamellar materials, the preparation involves, in general, three more steps after the introduction of the surfactant molecules: (i) the introduction of the pillaring agent which is responsible for the growth of interlamellar pillars, and (ii) the calcination process to obtain the pillared layered solid and, later, (iii) the grafting of the desired functional groups on the surface of this mesoporous solid. The pillarization of siliceous magadiite, to produce PILC-magadiites (Scheme 1), was shown by us in a previous publication.[2]

The results discussed here show the preparation of aminopropyl-functionalized mesoporous heterostructures in a single pot based on layered silicate (Scheme 1, HYB-magadiite), *i.e.*, the solids show characteristics of pillared layered silicates (Scheme 1, PILC-magadiite) and at the same time the properties of aminopropyl-grafted structures (Scheme 1, γ-magadiite).

3.1. γ-Magadiite: another part of the final hybrid

After demonstrating the effect of pillarization on the magadiite properties and in order to prove the individual features of each of the magadiite modifications, the surfaces of magadiite and

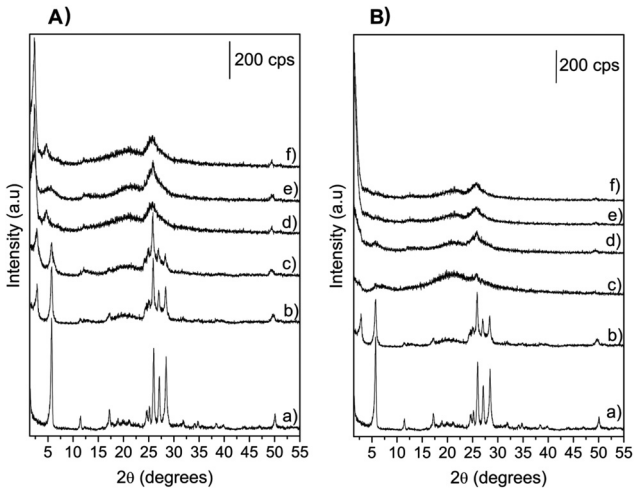

Fig. 1 X-ray diffractograms of functionalized magadiite (A): (a) magadiite; (b) CTA-maga28; (c) γ-maga28; (d) γ-maga61; (e) γ-maga88; and (f) γ-maga100. (B) X-ray diffractograms of functionalized [Al]-magadiites: (a) [Al]-magadiite; (b) CTA-[Al]-maga39; (c) γ-[Al]-maga39; (d) γ-[Al]-maga63; (e) γ-[Al]-maga72; and (f) γ-[Al]-maga99.

[Al]-magadiite were functionalized with γ-aminopropyl pending groups to understand the effect of the organofunctionalization alone, without pillaring influences.

After the CTA^+ exchange process (Fig. 1, curves b), confirmed by CHN analyses (See Table S1†), a 1.6 nm increase (in relation to Na-magadiite, curves a in Fig. 1) in the interlayer space was observed in all the samples (Fig. 1b shows the representative XRD of the lowest CTA concentration; for other values of the CTA/Na molar ratio see Fig. S1†). The basal spacing observed is close to the value expected on the basis of the molecular length of the surfactant with an interdigitated chain[23] at a 67.2° inclination in relation to the lamella (for details, see Fig. S2†), implying that basal spacing does not depend on the CTA/Na molar ratio in these cases.

The effect of the γ-aminopropyl groups on the long range order of the materials was examined by the X-ray diffractograms of CTA^+-magadiite and CTA^+-[Al]-magadiite. Fig. 1A and B show that the peaks in the range of 22–30° 2θ exhibit a significant decrease in intensity, indicating the loss of layer coherence. However, it is observed that the γ-magadiite solids (Fig. 1A, curves c–f) have a peak in the region of 2.3° 2θ (3.8 nm), indicating a basal spacing slightly larger than that observed for CTA^+-magadiite, probably needed to accommodate the pendant chains in the free space (Fig. 1A, curve b). A less evident situation occurs for [Al]-magadiite (Fig. 1B).

3.1.1. The organic part of γ-aminopropyl-magadiite and γ-aminopropyl-[Al]-magadiite. The characteristic vibrations of the magadiite and [Al]-magadiite structure can be observed in curves a in Fig. 2A and B. The bands between 1300 and 950 cm^{-1} are assigned to the antisymmetric stretching of the bonds on Si–O–Si moieties and symmetric stretching of $Si–O^-$ groups, respectively. Bands related to Si–O–Si stretching appear together at 821 and 789 cm^{-1}. The stretchings of Si–O–Si single and double rings present in the lamellar structure of magadiite are observed at 620 and 575 cm^{-1}.[24] Characteristic bands of organic groups are observed for CTA-magadiites and CTA-[Al]-magadiites (Fig. 2A and B, curves b): the C–H stretching between 3000 and 2800 cm^{-1} as well as the bands at 1475 cm^{-1}, assigned to the C–H deformation of methyl groups present in the polar head of the surfactant ($–N(CH_3)_3$ group), confirm the CTA^+ introduction into the magadiite interlayer space.

One can observe in the spectra of Fig. 2c–f (frames A and B for γ-magaX and γ-[Al]-magaX, respectively) an enlargement of the bands between 3000 and 2700 cm^{-1} (in relation to curves c) for the grafted samples due to the bands corresponding to the NH_2 groups that appear in the region of 3120 cm^{-1}, regardless of the concentration of CTA^+ present in the precursor. The band at 1380–1384 cm^{-1} in all samples (with various intensities) is assigned to the symmetric O–C–O stretching of ammonium carbamate formed by reaction of the pending groups with CO_2 from air.

The grafting process is accompanied by the loss of a part of the CTA^+ cations as proposed by Ogawa *et al.*[25] In this model (Fig. 3), the free silanol groups react with the organoalkoxysilane (in the case of Fig. 3, APTS) to form grafted silyl groups in the interlayer space with the generation of methanol (1). Methanol reacts with the neighboring silanol groups to form alkoxy groups and water (2). In (3), the generated water can interact with $CTA^+OSi\equiv$ sites to regenerate a silanol group. (4) The free silanol groups formed in step 3 react with the organoalkoxysilane as in step 1. After this process, a covalent bond is formed between the organoalkoxysilane and magadiite[25] and a large part of the CTA^+ is eliminated from the solid.

Fig. 4 shows the ^{13}C CP-MAS NMR spectra for the γ-aminopropyl-magadiite and γ-aminopropyl-[Al]-magadiite. The solids clearly present ^{13}C chemical shifts relative to aminopropyl groups linked to the layered material at 11, 24 and 44 ppm regions, corresponding respectively to the carbon attached directly to the silicon atom, the central carbon aminopropyl group and the carbon attached to nitrogen.[26] Although a part of the CTA^+ is lost in the process of grafting, the presence of residual cation is observed in the final material, in different conformations, when compared to the precursors CTA^+-magadiites (Fig. 4A and B, curves a). A resonance appears at 128 ppm for γ-[Al]-maga63 and γ-[Al]-maga99 assigned to C=C bonds,[27] coming from 1-hexadecene,[28] a product from the Hoffman degradation of CTA^+.

When aminopropyl groups are added to the solid, carbon resonances are broader and slightly shifted with respect to those of CTA-magadiite precursors. This suggests that the carbon atoms of CTA are anisotropically distributed in different environments.[29] Detailed information regarding the structure and dynamics of the CTA^+ molecules in magadiite samples were obtained recently by Pastore *et al.*[30] Surfactant molecules may assume mixed conformations because of the balance among several effects: attractive forces between the

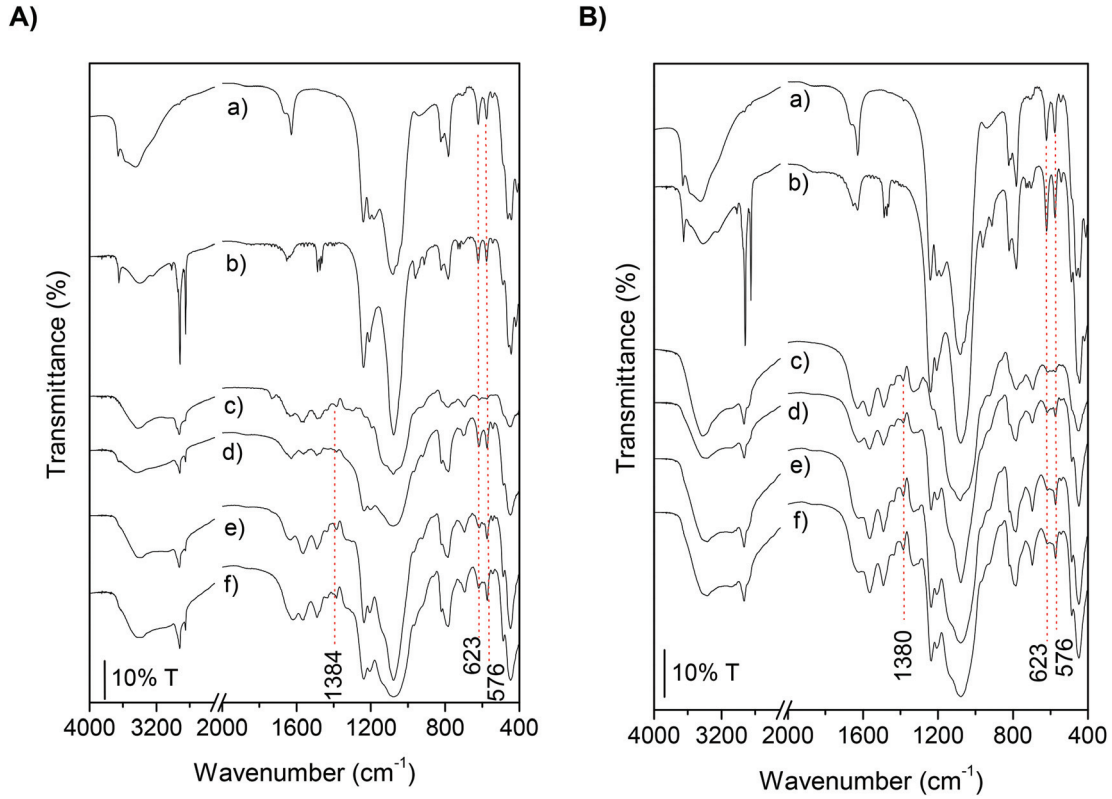

Fig. 2 FT-IR spectra of aminopropyl grafted (A) magadiite: (a) magadiite; (b) CTA-maga28; (c) γ-maga28; (d) γ-maga61; (e) γ-maga88; and (f) γ-maga100. And (B) [Al]-magadiites: (a) [Al]-magadiite; (b) CTA-[Al]-maga39; (c) γ-[Al]-maga39; (d) γ-[Al]-maga63; (e) γ-[Al]-maga72; and (f) γ-[Al]-maga99.

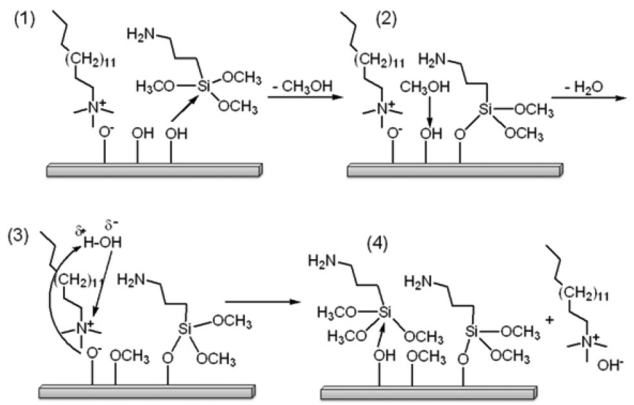

Fig. 3 Grafting of organoalkoxysilane (APTS) to the interlamellar surfaces of magadiite. Adapted from Ogawa *et al.*[25]

heads of alkylammonium cations (CTA^+ and APTS) and the silicate surface, repulsive forces between the alkyl chains and the silicate surface and van der Waals interactions between alkyl chains.

A peak at 164 ppm, assigned to the carbamate formation (already observed on FTIR), is present in the materials, indicating their possible use as a CO_2 scavenger.

3.2. The hybrids HYB-magadiite and HYB-[Al]-magadiite

The knowledge of the effects of SiO_2-pillaring[2] and γ-aminopropyl grafting on magadiite and [Al]-magadiite allows envisaging the effect of the simultaneous changes in the solids, discussed in the next sections.

3.2.1. Order at long distances. Regardless of the presence or absence of aluminum in the framework, the peak at 2.8° 2θ, assigned to the basal spacing of CTA-magadiite,[8] is not observed after modification with TEOS and APTS (Fig. 5A and B, curves b to e); it is substituted by a peak at higher angles (from 5.70° to 6.40° 2θ for magadiite and from 4.98 to 6.24° 2θ for [Al]-magadiite) as the CTA/Na molar ratio increases in the precursor (Table S2†), coherent with the CTA^+ elimination from the interlayer space during pillar growth, already commented.

During the process of synthesis of the hybrid material, curves b–e from Fig. 5A and B show that the turbostratic effect and loss of lamella coherence, already present in CTA-maga28 and CTA-[Al]-maga39 (curves a, Fig. 5), become more accentuated after the pillaring/functionalization process as commented before for γ-magaX and γ-[Al]-magaX. The XRD of these samples shows an amorphous halo in the range of 22–30° 2θ still keeping a weak signal at 26° 2θ from the lamella structure. In the case of the hybrids HYB-magaX and HYB-[Al]-magaX,

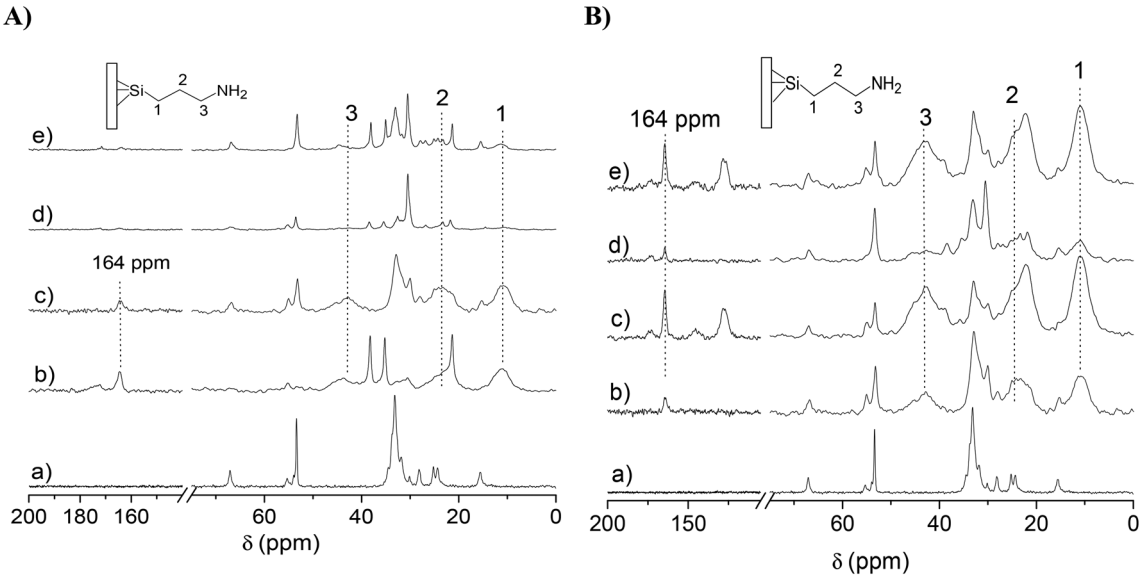

Fig. 4 $^{13}C\{^{1}H\}$ CP MAS NMR spectra of aminopropyl grafted (A) magadiite: (a) CTA-maga28, (b) γ-maga28, (c) γ-maga61, (d) γ-maga88 and (e) γ-maga100. (B) [Al]-magadiites: (a) CTA-[Al]-maga39, (b) γ-[Al]-maga39, (c) γ-[Al]-maga63, (d) γ-[Al]-maga72 and (e) γ-[Al]-maga99.

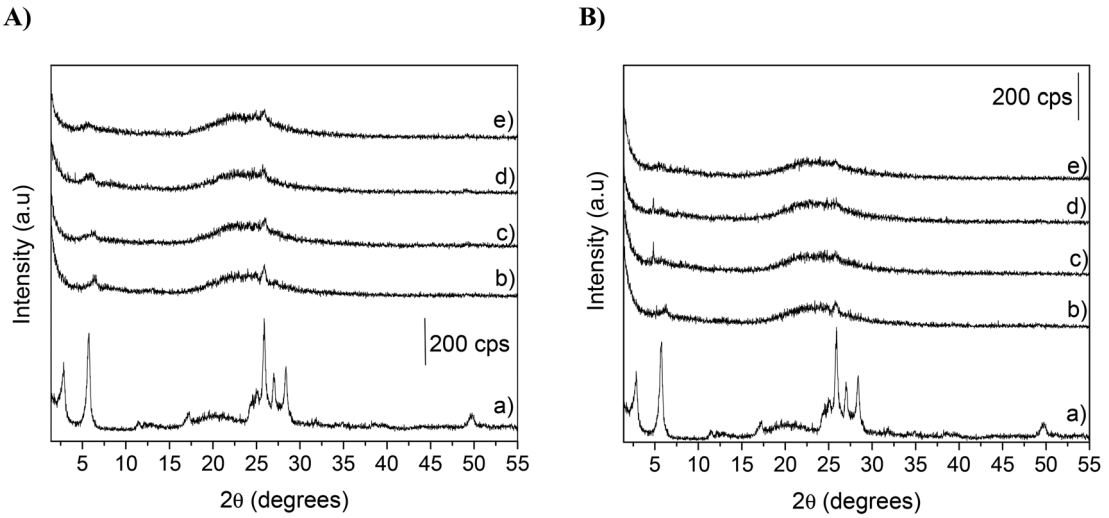

Fig. 5 X-ray diffractograms of hybrid materials derived from magadiite (A): (a) CTA-maga28; (b) HYB-maga28; (c) HYB-maga61; (d) HYB-maga88; and (e) HYB-maga100. (B) X-ray diffractograms of hybrid materials derived from [Al]-magadiites: (a) CTA-[Al]-maga39; (b) HYB-[Al]-maga39; (c) HYB-[Al]-maga63; (d) HYB-[Al]-maga72; and (e) HYB-[Al]-maga99.

the disorganization and the formation of the halo are much more pronounced than in the case of γ-magaX and γ-[Al]-magaX (compare Fig. 1 and 5).

These differences indicate that the formation of the pillars affects the layered material in two ways: causing disorganization and increasing the turbostratic effect and introducing a portion of amorphous silica as pillars. The fact that the first intense peak of swollen samples was not observed is due to the fact that the diffraction object is very small to the X-rays; therefore poor diffraction is observed. SAED (Fig. 6B) confirms that the crystallinity of the magadiite lamella is preserved with the appearance of two clear diffraction patterns, one slightly shifted from the other. If one considers the lamella stacking as occurring in the *c* direction, these patterns seem to indicate that the layers shifted by the introduction of pillars in the *a*, *b* or *a* and *b* directions. That is the reason for the absence of X-ray diffraction signals.

3.2.2. The molecular structure of the hybrids: FTIR and NMR. The mesoporous hybrids, also evaluated by FTIR (Fig. S3A and B,† curves a), show the characteristic vibrations of the magadiite structure between 1300 and 400 cm^{-1} described before for CTA-magadiite.[2]

After hybrid formation, curves b–e on Fig. S3A and B† show that the bands related to the double rings characteristic of the

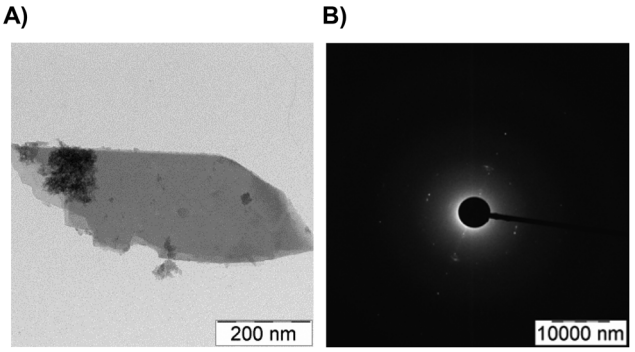

Fig. 6 (A) Transmission electron microscopy (TEM) and (B) selected area electron diffraction (SAED) of calcined HYB-maga28.

lamella crystal structure of the material in 577 and 618 cm^{-1} are preserved. Despite the decrease of the relative intensity of these bands with the modifications, their presence in the hybrids indicates that the structure of the magadiite lamella was preserved. The comparison of Fig. 2 and Fig. S3† shows that the preservation of the bands due to the double rings typical of the magadiite structure is more important in γ-magaX and γ-[Al]-magaX than in HYB-magaX and HYB-[Al]-magaX probably because of the presence of amorphous pillars in the material and the decrease of the relative amount of crystalline solid.

Fig. S3A and B† also show a weak band in all hybrids (with various intensities) at 1382 cm^{-1} assigned to the symmetric stretching O–C–O due to the formation of ammonium carbamate, as commented for the grafted γ-magaX and γ-[Al]-magaX. The hybrid materials also display the loss of CTA^+ upon pillaring/functionalizing/grafting process in the same way as shown for the grafted materials (Fig. 3).

Local order in such hybrid solids was also evaluated by nuclear magnetic resonance of ^{29}Si nucleus. The curves in Fig. 7A and B show the ^{29}Si NMR spectra of the silicates after insertion of TEOS and APTS. Besides the presence of sites Q^3 and Q^4 typical of magadiite pillared with TEOS, in the region of −90 to −100 ppm,[2] signals of T^2 and T^3 sites (region of −60 ppm) were observed, indicating the insertion not only of TEOS but also the aminopropyl group in the lamellar structure, showing the formation of a hybrid. There is a tendency of the percentage of T sites to increase in relation to Q sites when the CTA^+ concentration in the solid precursor is higher (Table S3† shows the Si_T/Si_Q ratios of the hybrid materials and also their unit cell). That is, according to the mechanism in Fig. 3, $CTA^+OSi\equiv$ sites on the magadiite surface are more available in the presence of larger amounts of CTA^+ in the precursor, allowing higher degrees of incorporation of functional groups.

The ^{13}C NMR spectra of these hybrids present chemical shifts relative to the aminopropyl groups (Fig. S4†) already observed in γ-magaX and γ-[Al]-magaX exclusively. During the synthesis of these hybrids derived from magadiite and [Al]-magadiite, the ^{27}Al NMR spectra (Fig. 8) show the maintenance of signals at 53 and 6 ppm regions assigned to species of aluminum in tetrahedral and octahedral coordination, respectively.[30]

The scanning electron microscopy images of both magadiite and [Al]-magadiite hybrid materials synthesized are similar to clays as already observed for aminopropyl-modified magnesium–phyllosilicates[26] (Fig. S5† presents only HYB-[Al]-magaX due to the similarities to HYB-magaX).

In summary, compared with the published features of pillared magadiites,[8] it is observed that TEOS (or TEOS and APTS) produces firm enough silica-pillars to prop the expanded gallery after the removal of surfactants. In this step, the X-ray diffractogram shows that the signals in the region of 22–30° 2θ are substituted by an amorphous halo, typical of disorganized material. In spite of this disorganization, the lamella or small groups of lamellas have their crystallinity

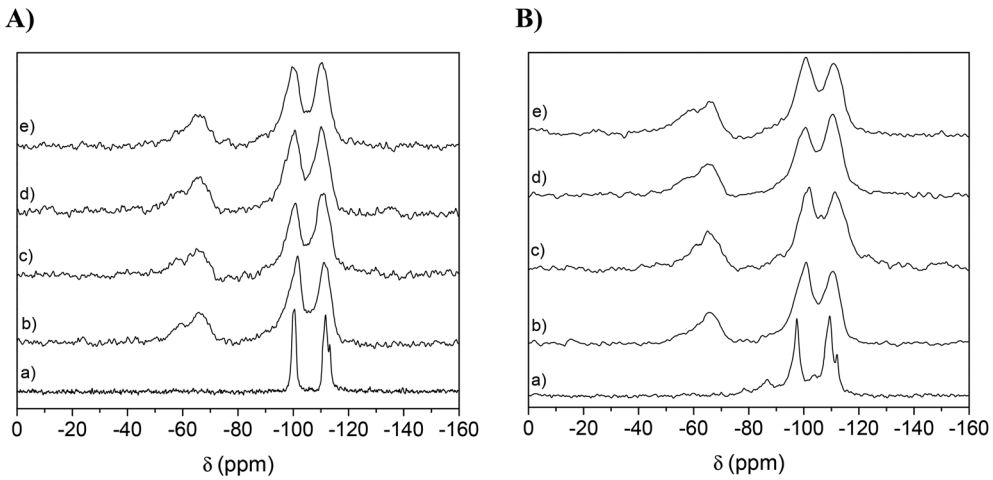

Fig. 7 ^{29}Si NMR spectra of hybrid materials derivated from magadiite (A): (a) Na-magadiite; (b) HYB-maga28; (c) HYB-maga61; (d) HYB-maga88; and (e) HYB-maga100. (B) ^{29}Si NMR spectra of hybrid materials derivated from [Al]-magadiites: (a) Na-[Al]-magadiite; (b) HYB-[Al]-maga39; (c) HYB-[Al]-maga63; (d) HYB-[Al]-maga72; and (e) HYB-[Al]-maga99.

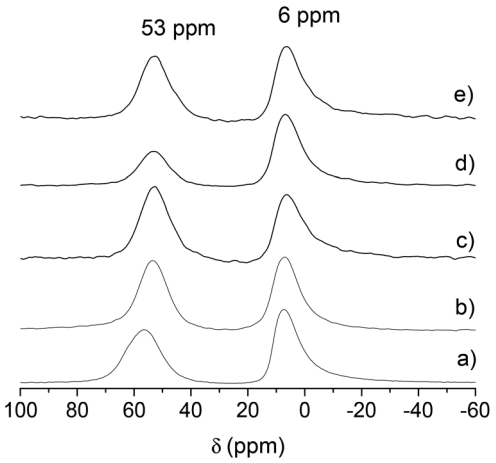

Fig. 8 ^{27}Al NMR spectra of hybrid materials derived from [Al]-magadiites: (a) Na-[Al]-magadiite, (b) HYB-[Al]-maga39, (c) HYB-[Al]-maga63, (d) HYB-[Al]-maga72 and (e) HYB-[Al]-maga99.

preserved, as shown by both FTIR and SAED/TEM. ^{29}Si NMR allowed us to conclude that the organic groups are bound to the solid as proposed by the presence of T sites along with Q^3 and Q^4.

3.2.3. General effects on porosity. The success of the pillaring process is confirmed by significant variations in the surface area and pore size. Fig. 9 shows that adsorption and surface area of magadiite and [Al]-magadiite are very low, typical of layered solids. The N_2 adsorption–desorption isotherms of the non-calcined HYB-maga28 and HYB-[Al]-maga39 solids are shown and compared to the grafted and pillared forms in Fig. 9 while the data on surface area, pore volume and pore size of these hybrids are shown in Table S4.†

The HYB-magadiites and HYB-[Al]-magadiites display an increase in porosity and in the surface area (values between 49–61 and 38–60 $m^2\ g^{-1}$, respectively) when compared to the starting material (25 $m^2\ g^{-1}$ for magadiite and 32 $m^2\ g^{-1}$ for [Al]-magadiite) better envisaged in Fig. S6.† This is probably due to the fact that TEOS, as the pillaring precursor, is converted to silica pillars and forms the rigid intercalated porous structure as in the case of pillared magadiite[8] and [Al]-magadiite. The surface area is not as large as in the case of pillared solids (512 $m^2\ g^{-1}$ for PILC-maga28 and 641 $m^2\ g^{-1}$ for PILC-[Al]-maga39), probably due to the fact the organic groups still populate the pores in HYB-magadiites and in HYB-[Al]-magadiites, but it is similar to the amino-grafted materials (Table S4,† 74 $m^2\ g^{-1}$ for γ-maga28 and 67 $m^2\ g^{-1}$ for γ-[Al]-maga39), indicating that HYB-magaX and HYB-[Al]-magaX are pillared and grafted solids, obtained in a single step synthesis.

At this point, the effects of simultaneous SiO_2-pillaring and of γ-aminopropyl-grafting on magadiite and on [Al]-magadiite confirmed that the surface properties of layered silicates can be designed by controlling the degree of silylation/pillarization.

3.2.4. Interlayer pillar growth: a factual 3D structure. PILCs present, in general, lower structural regularity than zeolites, but are more organized than other important classes of adsorbent materials. Therefore, the lack of a zeolitic-type, precise, regular structure cannot be regarded as a disadvantage for PILC applications as adsorbents. As a matter of fact, particular attention is devoted also to the potentialities of PILCs as selective adsorbents of natural and biogas components, such as carbon dioxide, methane, ethane, and nitrogen. While the gallery heights of the CTA^+-intercalated solids can usually be known with high accuracy from X-ray diffraction, the knowledge of the volume between the pillars poses more difficulties.[31]

The use of particular organic molecules, such as surfactants, in the pillaring solution to act as a swelling agent has been studied before.[32] It involves the introduction of an organic molecule into the interlayer space along with the pillaring species. The organic molecule, of known shape and size, can later be removed by calcination to leave a more regular pore structure. By investigating how such organic

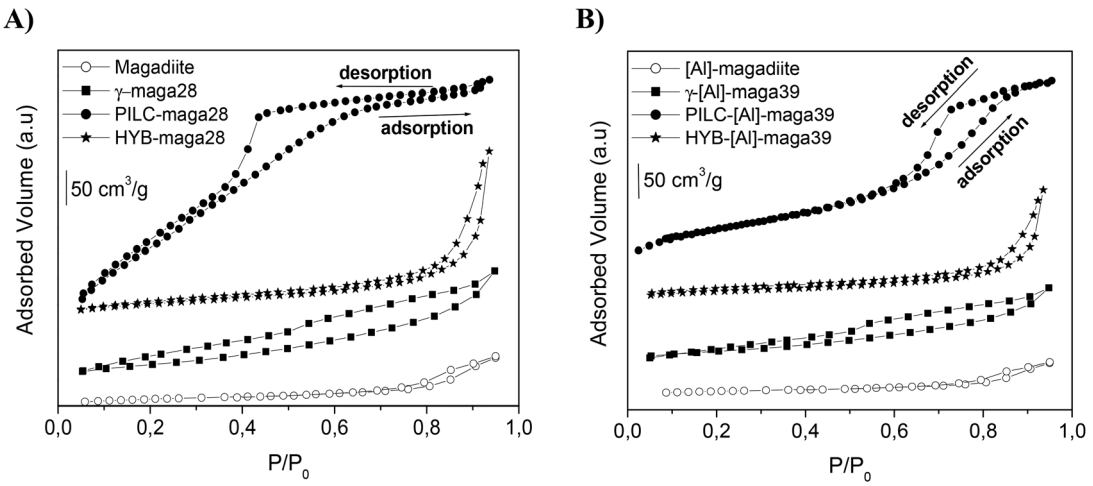

Fig. 9 N_2 adsorption–desorption isotherms of non-calcined modified magadiite (A) and [Al]-magadiite (B). (Isotherms are displaced by 148 $cm^3\ g^{-1}$ to HYB-maga28/[Al]-maga39, 50 $cm^3\ g^{-1}$ to γ-maga28/γ-[Al]-maga39 and 187 $cm^3\ g^{-1}$ to PILC-maga28/[Al]-maga39.)

molecules affect the pillaring process, specific pore sizes can be designed. Michot and Pinnavaia[33] incorporated a non-ionic surfactant of general formula $C_{12-14}H_{25-29}O(CH_2CH_2O)_5$ into the usual Al-pillaring solution. The resulting PILC had a more uniform micropore distribution and a sharper and more symmetrical 001 reflection compared to the one prepared without a surfactant. The basal spacing (15.3 Å) was, however, smaller than the procedure effected in the absence of a surfactant (17.8 Å); this was attributed to the surfactant limiting the condensation of Al_{13} units within the interlayer space. The surface area (305 $m^2\ g^{-1}$) was also slightly larger than the conventional PILC (279 $m^2\ g^{-1}$) and the solid was found to contain more mesopores.

Using 3-aminopropyltrimethoxysilane (APTS) and 2-(2-trichlorosilylethyl)pyridine (TCSEP) as pillaring agents, Fetter and others[34] produced two different pillared clays with good thermal stability. The microporous volume of TCSEP-PILC was 0.15 $cm^3\ g^{-1}$ and 0.186 $cm^3\ g^{-1}$ for APTS-PILC. These Si-pillared clays show a small number of weakly acidic sites and some strongly acidic sites retaining ammonia up to 723 K, which are most likely localized on the clay lamella.

One of the main questions posed when an interlayer pillared lamellar material is presented concerns the real composition of phases, pillaring and lamella, and bonding between them at the molecular scale. Due to the heterogeneous nature of the reactions, the possibility of having a physical mixture of the unchanged layered material and an amorphous phase derived from the pillaring reactants has to be always taken into account. The fact that the amorphous pillars are generally in a much larger concentration does not make the assessment any easier. In the present case, the fact that the layered material is a crystalline silica (or aluminosilicate) and the pillars are amorphous silica does not represent the best possible situation in terms of characterization.

The main physical technique to tell about bonding between these two phases, the ^{29}Si-NMR, is not adapted to the case where one phase is crystalline and the other is amorphous of essentially the same composition. Therefore, several chemical tests were performed in order to get more insight into the nature of the solids prepared in this work and the interaction of the phases that compose them.

To better envisage the proposed interlayer pillarization, sample HYB-maga28 was compared to a solid that is composed of an amorphous silica phase mechanically mixed with crystalline CTA-magadiite. First, TEOS and APTS, the pillaring agents, were pre-hydrolyzed exactly as performed in the synthesis of HYB-maga28. The solid obtained was named "hydrolyzed TEOS + APTS". Then, hydrolyzed TEOS + APTS and CTA-maga28, in the same molar ratio as for the preparation of HYB-maga28, were thoroughly mixed in a mortar and named MIX.

Fig. 10 presents the XRD of these solids. Na-magadiite (a), CTA-maga28 (b) and H-magadiite (c) were also plotted for comparison. The hydrolyzed TEOS + APTS (curve d) is a typical amorphous solid. When this solid is mixed with CTA-maga28 (curve b), yielding MIX (curve e), one obtains a physical

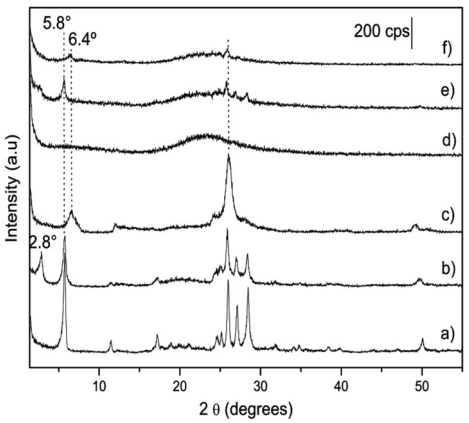

Fig. 10 X-ray diffractograms of (a) Na-magadiite, (b) CTA-maga28, (c) H-magadiite, (d) hydrolyzed TEOS + APTS, (e) mixture of hydrolyzed TEOS + APTS and CTA-maga28 (MIX) and (f) HYB-maga28.

mixture: the signals of both CTA-maga28 and of hydrolyzed TEOS + APTS are clearly observed, and no variation in either position or relative intensity can be indicated. Even the small intensity signal around 50° 2θ due to CTA-maga28 can be observed in MIX (Fig. 10, curve e).

These observations help clarify the features observed in a physical mixture of CTA-maga28 and an amorphous silica phase. Curve f in Fig. 10 displays the powder X-ray diffractograms of the silica-pillared aminopropyl-grafted magadiite. The differences between curves f and e, of the MIX, are clear. The crystalline counterpart seems to be of lower importance than in the physical mixture. Moreover, it seems to be the profile of H-magadiite (curve c), not of CTA- or Na-magadiite. The fact that the peak at 2.8° 2θ in CTA-magadiite disappears upon pillarization and not upon physical mixing is revealing: it indicates that the difference between HYB-maga28 and MIX is that, in the first case, the pillarization reaction occurs in the same interlayer space where the CTA^+ is located and not in the interlayer spaces where CTA^+ has not ion exchanged Na^+. In these spaces, however, grafting might have occurred because one obtains the H-magadiite profile, and not Na-magadiite.

The second aspect is that in order that the silica precursors arrive at the interlayer spaces and do not generate a separated silica phase, it is necessary that the species in reaction have the dimensions of small oligomers at maximum. To begin this part of the investigation, the pillaring solution composed of hydrolyzed TEOS and APTS was investigated by ^{29}Si liquid state NMR (Fig. 11). It is worth remembering that this solution is exactly the one that gets in contact with CTA-maga28 for pillaring. Species at −88.5 and −81.7 ppm are assigned to Q^2 in linear and in cyclic trimers (Q^2_Δ),[35] respectively. Two resonances around −53 ppm are assigned to $(NH_2(CH_2)_3)Si(OSi)(OH)_2$ from T sites and a peak at −45 ppm corresponds to the chemical shift of Si in liquid APTS, thus indicating the presence of free silylating molecules in the solution.[36] Free TEOS was not observed in solution probably because it hydrolyses first. That is, when the crystalline CTA-maga28 is added to the

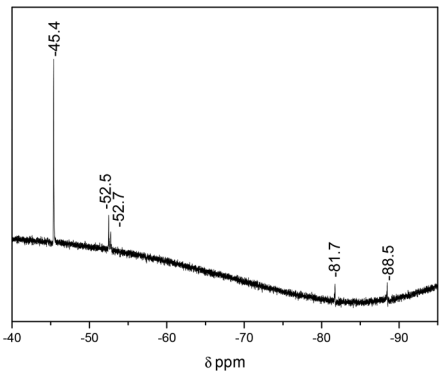

Fig. 11 ^{29}Si liquid state NMR of the pillaring solution containing TEOS + APTS. The signal due to the glass tube appears at a region lower than −100 ppm.

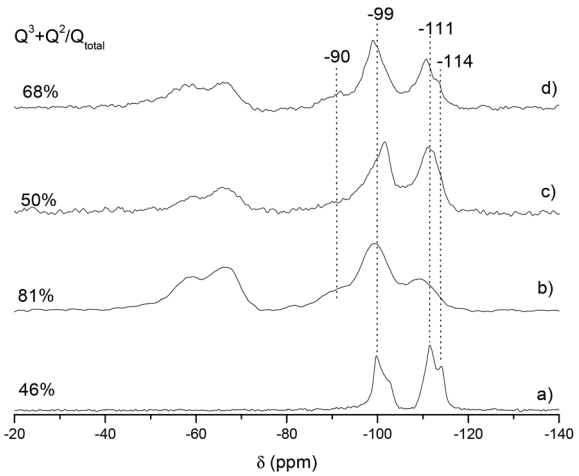

Fig. 12 ^{29}Si HPDEC NMR spectra of (a) CTA-maga28, (b) hydrolyzed TEOS + APTS, (c) HYB-maga28 and (d) mixture of hydrolyzed TEOS + APTS and CTA-maga28 (MIX).

synthesis, the Si species are not completely polymerized; thus, these species are able to migrate to the interlayer space of CTA-magadiite and condense there.

The ^{29}Si NMR of the solids (Fig. 12) can be analyzed from two points of view. Hydrolyzed TEOS + APTS (curve b) and MIX-sample (curve d) both show signals at around −90 ppm and a reasonably more intense Q^3 peak at *ca.* −99 ppm, indicating highly depolymerized, hydroxylated silica surfaces. These conclusions are supported by the $Q^3 + Q^2/Q_{total}$ ratios, and these two compounds present the highest values among the samples tested. The 4% difference of $Q^3 + Q^2/Q_{total}$ between CTA-maga28 (curve a) and HYB-maga28 (curve c) can be assigned to the amorphous silica pillars in HYB-maga28. Also, the presence of Q^4 sites, typical of CTA-maga28 at −114 ppm (curve a), is much more evident in the case of the mixed amorphous and crystalline phases (curve d) than in the case of HYB-maga28 (curve c). In other words, a simple mechanical mixture of amorphous pillars and crystalline magadiite (curve d) does not disturb the magadiite framework as it does when the pillar is linked to the lamella (curve c): the peak corresponding to Q^4 is less pronounced.

At this point it is possible to conclude that HYB-maga28 is indeed an individual material in itself; it is not the mixture of CTA-magadiite and amorphous hydrolyzed TEOS + APTS or CTA-magadiite tactoids surrounded by amorphous silica. To further support these conclusions, the porosity of these materials was examined.

Comparing the N_2 adsorption/desorption properties of the solids from Fig. 13, one observes that magadiite (Fig. 13A and A′) presents a large pore size distribution in the range of 15–22 nm assigned to pores formed from aggregation of particles, the secondary pore system. The same is observed for CTA-maga28: a secondary large pore system due to aggregation of particles. This indicates that ion exchange with CTA^+ does not alter the particles enough to create a new arrangement of aggregation. However, in CTA-maga28 a new mesopore system appears in the range from 5 to 10 nm, the highest density around 5.99 nm that did not exist in magadiite. The mesopore system in the sample is the space where pillars will be built. A small population of pores appears at 10.5 nm and another one at 15.0 nm.

When the CTA-maga28 is physically mixed with the aminopropyl modified amorphous silica (Fig. 13, curves C and C′), what one observes is an unspecific uprising of the baseline in the range from 3.6 to 15.0 nm. The maxima observed in this situation are 4.85 and 6.80 nm, these contributions have to come from the amorphous material. One important feature is that the secondary pore system at high P/P_0 observed in magadiite and CTA-maga28 is not observed in the MIX-sample (Fig. 13C′). If HYB-maga28 were simply a mixture as the MIX-sample, the profile in Fig. 13D′ would be the same as Fig. 13C′, and it is not. In Fig. 13D′, the structural mesopore system appears at 4.88 nm with a tail extending up to *ca.* 10.0 nm. In this case, narrower pores are formed in comparison to the pores observed in CTA-maga28, meaning that less space is available for N_2 after the introduction of APTS-functionalized pillars. However, HYB-maga28 does show a certain degree of porosity (~4–13 nm) due to the access of N_2 to the interlayer space. One has to remember that 26% of the total silicon bears a pending group (see Table S3†).

In broad terms, the general profile of HYB-maga28 is similar to CTA-maga28: one mesopore system peaking between 4 and 6 nm tailing until 10 nm. Aggregation pores are observed at around 20 nm. The system observed at 10.5 nm in CTA-maga28 probably generates another pore system in HYB-maga28 at 11.4 nm. Calcination of HYB-maga28 (Fig. 13E′) freezes two mesopore systems, both displaying a distribution of pore sizes around 5.0 and 8.5 nm.

3.3. Improved CO_2 adsorption capacity

There are several studies on the adsorption of carbon dioxide on γ-aminopropyl groups grafted on porous silicate surfaces; therefore, the HYB-solids were investigated in order to evaluate the effects of their porosity on CO_2 adsorption properties. To

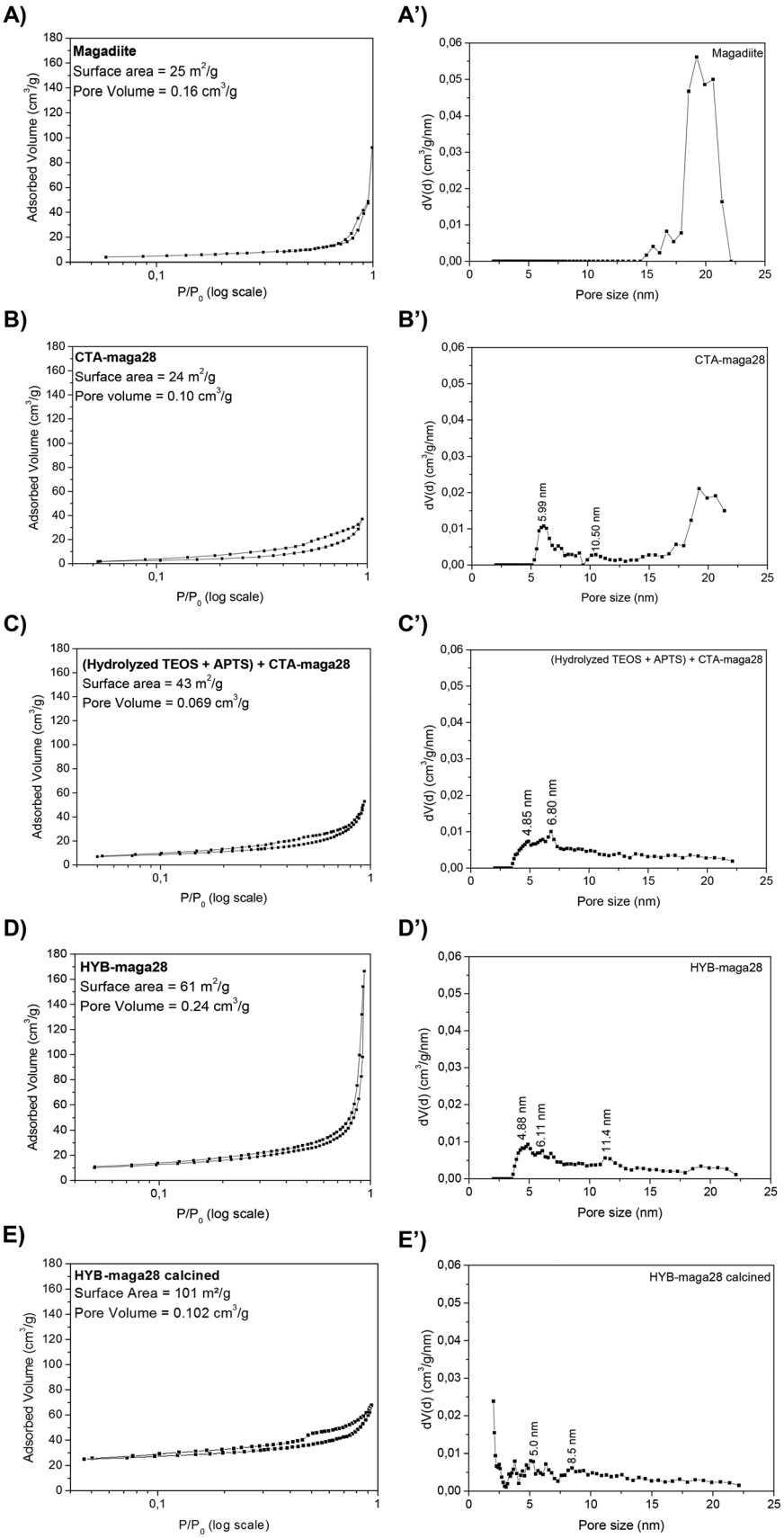

Fig. 13 N_2 adsorption/desorption isotherms of (A) Na-magadiite, (B) CTA-maga28, (C) mixture of hydrolyzed TEOS + APTS and CTA-maga28 (MIX), (D) HYB-maga28 and (E) calcined HYB-maga28 and their respectively pore size distribution (').

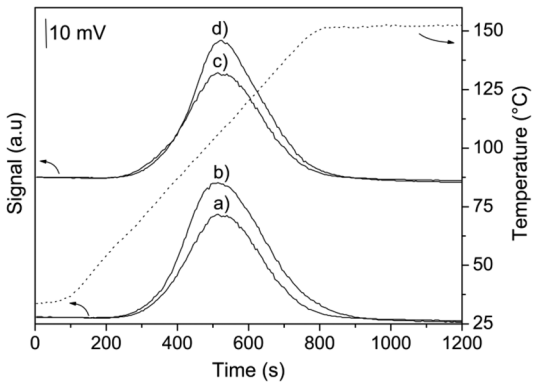

Fig. 14 Temperature-programmed of CO_2 desorption on (a) γ-maga28, (b) HYB-maga28, (c) γ-[Al]-maga39 and (d) HYB-[Al]-maga39. (Curves c and d are displaced from a and b by 50 mV.)

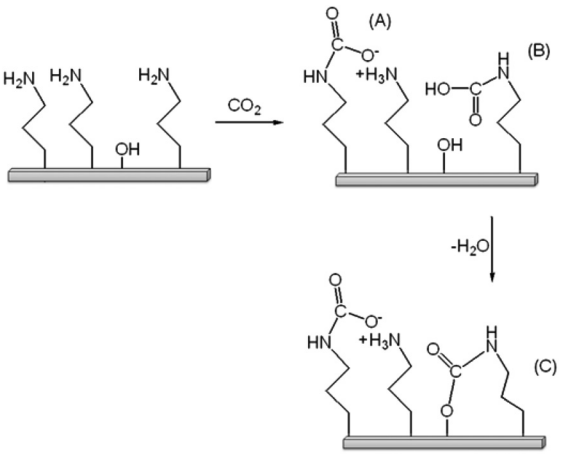

Scheme 2 Schematic representation of the CO_2 adsorption on amino-propyl-modified solids.

demonstrate the improved properties of the hybrid materials in relation to the pillared[8] and to the aminopropyl-grafted magadiites shown here, after a dehydration step, the solids were exposed to the CO_2/He (5%) atmosphere at 50 °C (previously determined as the best adsorption temperature) and the desorption curves are shown in Fig. 14.

The solids HYB-maga28 and HYB-[Al]-maga39 displayed a significant improvement in carbon dioxide efficiency when compared to the γ-maga28 and γ-[Al]-maga39. The increase was *ca*. 60%: from 0.37 to 0.60 CO_2/N for HYB-maga28 and from 0.46 to 0.65 CO_2/N for HYB-[Al]-maga39 (Table S5†). The low CO_2 adsorption by γ-maga28 and γ-[Al]-maga39 is the result of the closeness of the lamella brought forth by the dehydration process, hindering the CO_2 diffusion to the anchoring sites in the pending groups. In the case of HYB-maga28 and HYB-[Al]-maga39, lamellas are firmly separated from each other due to the presence of pillars between them and, thus, cannot collapse. As a result, the CO_2 access to the $-NH_2$ groups in these materials is more effective, *i.e.*, the HYB-magaX and HYB-[Al]-magaX can make use of the amino groups functionality to adsorb CO_2 and hence the increase in CO_2/N ratios observed.

For the hybrid materials, the efficiency is higher than 0.5, the value predicted by the stoichiometry of the alkylcarbamate formation. This is probably due to CO_2 simultaneous adsorption to $-NH_2$ and surface SiOH groups,[37] which increases the efficiency to values above 0.5 and was already observed for amino-functionalized talcs.[38]

Aminopropyl-modified silicas absorb CO_2 as mainly propylammonium propylcarbamate (Scheme 2, species A), propylcarbamic acid (Scheme 2, species B), and propylammonium silylpropylcarbamate (Scheme 2, species C). As proposed by Weitz *et al.*,[31] if the propylamine group density is high enough, ammonium carbamate ion pairs are the main species observed (species A in Scheme 2). The more isolated aminopropyl groups tend to form propylcarbamic acid, preferentially (species B in Scheme 2). This species interacts with the surface OH groups, if they exist in a large number, to produce a stable surface-bound carbamate and release water molecules (species C in Scheme 2); these species increase the efficiency for the materials to values above 0.5.

Table 1 Calculated occupied surface area by $-NH_2$ groups

	$-NH_2$ group content (mmol g^{-1})	Surface area (m^2 g^{-1})	Occupied surface area[a] (m^2 g^{-1})
γ-maga28	0.276	74	7.5
γ-[Al]-maga39	0.232	67	6.3
HYB-maga28	0.220	61	5.9
HYB-[Al]-maga39	0.196	60	5.3

[a] = ($-NH_2$ content) × (Avogadro's constant) × (NH_2 polar head area). NH_2 polar head area was estimated as 0.045 nm^2 per molecule using Gaussian View 5.0.

Table 1 shows the surface areas measured by N_2 adsorption at low temperatures and the estimated values of the surface area occupied by the pending groups on these solids. The calculation of surface occupation by the pending groups (3rd column in Table 1) is only approximately 10% of the total area; therefore low amine densities were obtained and neighbouring amine groups are not frequent.

Regardless of the presence of aminopropyl groups, the insertion of aluminum into the magadiite layers generates Bronsted and Lewis acid sites. CO_2 can interact with the heteroatom, in a Lewis acid–base type interaction by a mechanism similar to that proposed by Weitz *et al.*,[39] and produce mono and bidentated carbonates. Solids capable of this type of interaction display increased CO_2 adsorption.

4. Conclusions

The intercalation of different concentrations of CTA^+ cations and subsequent pillaring by TEOS and APTS hydrolysis into magadiite and [Al]-magadiite interlayer space resulted in a mesoporous material with significant variation in surface

areas and pore sizes and containing functional aminopropyl groups.

The magadiite and [Al]-magadiite basic sheets are maintained as evidenced by FT-IR. The pillaring process caused a loss of coherence of the pillaring of magadiite layers in such a manner as to cause the disappearance of the diffractions due to interaction with X-rays. The electron diffraction, however, detected the crystalline hybrid, in the XRD-amorphous solid, where the lamellas were slightly shifted one from the other, confirming the FTIR short distance organization.

Aminopropyl-grafted structures, γ-magaX and γ-[Al]-magaX, have $-NH_2$ pending groups available for CO_2 capture but showed discrete values in adsorption due to the closeness of the lamella after the dehydration process. On the other hand, in SiO_2-pillared silicates, pillars between the lamella avoid their collapse and are responsible for larger surface areas and accessible pores, but the CO_2 adsorption is restricted to the SiOH groups. According to these results, the effects of simultaneous SiO_2-pillaring and γ-aminopropyl grafting on magadiite and [Al]-magadiite were combined, generating the hybrid solids (HYB-magaX and HYB-[Al]-magaX) which possess the pores and pillars properties of the pillared solids and the CO_2 improved adsorption properties from aminopropyl-grafted magadiite and [Al]-magadiite (*ca*. 60%).

The knowledge of the effects of SiO_2-pillaring and grafting on layered silicates allows envisaging the effect of the simultaneous changes in the solids. Using magadiite and [Al]-magadiite, aminopropyl-functionalized mesoporous heterostructures with designed pore structure, accessibility and activity can be obtained in a single step synthesis, as reported in the present work. These hybrid materials consisted of magadiite and [Al]-magadiite pillared with TEOS–APTES 1 : 1 (HYB-magadiites and HYB-[Al]-magadiites) and display an increase in porosity and in the surface area (values between 49–61 and 38–60 $m^2\ g^{-1}$, respectively) when compared to the starting material (25 $m^2\ g^{-1}$ for magadiite and 32 $m^2\ g^{-1}$ for [Al]-magadiite). The surface area is not as large as in the case of SiO_2-pillared solids (512 $m^2\ g^{-1}$ for magadiite and 641 $m^2\ g^{-1}$ for [Al]-magadiite), probably due to the fact that the organic groups populate the pores, but it is similar to the amino-grafted materials (74 $m^2\ g^{-1}$ for aminopropyl-grafted magadiite and 67 $m^2\ g^{-1}$ for NH_2-grafted-[Al]-magadiite), indicating that the hybrids proposed are simultaneously pillared and grafted solids and not a simple mixture of crystalline and amorphous phases.

All these results point to the same situation: magadiite and [Al]-magadiite can be pillared giving pores with variable volumes by careful control of the CTA/Na molar ratios in the initial swelling step. The processes of grafting aminopropyl groups directly to the lamella (γ-maga and γ-[Al]-maga) or of pillaring with TEOS only (PILC-maga and PILC-[Al]-maga) produce materials that are not good CO_2 adsorbents either because the lamella are very close after dehydration (the γ-maga and γ-[Al]-maga) or because they do not have the functional groups (the PILC-maga and PILC-[Al]-maga). The pillaring process by the mixture of TEOS and APTS causes the loss of coherence of the lamella; however, the CO_2 capacity increases considerably, indicating that the pillars are really capable of keeping the lamella apart, increasing the access of the CO_2 molecules to the interlayer space.

Acknowledgements

The authors are grateful to Petrobras for the scholarship granted and financial support of this work. The Fundação de Amparo à Pesquisa do Estado de São Paulo (FAPESP) is acknowledged for the instruments used in this work (2008/00132-6). The Conselho Nacional para o Desenvolvimento Científico e Tecnológico, CNPq, is acknowledged for the fellowship (HOP).

Notes and references

1 A. Gil, S. A. Korili, R. Trujillano and M. A. Vicente, *Appl. Clay Sci.*, 2011, **53**, 97.
2 J. Pires, A. C. Araujo, A. P. Carvalho, M. L. Pinto, J. M. Gonzalez-Calbet and R. Castellanos, *Microporous Mesoporous Mater.*, 2004, **73**, 175.
3 M. Polverejan, T. R. Pauly and T. J. Pinnavaia, *Chem. Mater.*, 2000, **12**, 2698.
4 A. Galarneau, A. Barodawalla and T. J. Pinnavaia, *Nature*, 1995, **374**, 529.
5 M. Nakatsuji, R. Ishii, Z. M. Wang and K. Ooi, *J. Colloid Interface Sci.*, 2004, **272**, 158.
6 M. Pichowicz and R. Mokaya, *Chem. Commun.*, 2001, 2100.
7 R. Ishii, M. Nakatsuji and K. Ooi, *Microporous Mesoporous Mater.*, 2005, **79**, 111.
8 H. M. Moura, F. A. Bonk and H. O. Pastore, *Eur. J. Mineral.*, 2012, **24**, 903.
9 R. Ishii, T. Ikeda, T. Itoh, T. Ebina, T. Yokoyama, T. Hanaoka and F. Mizukami, *J. Mater. Chem.*, 2006, **16**, 4035.
10 P. Ferreira, C. D. Nunes, J. Pires, A. P. Carvalho, P. Brandao and J. Rocha, *Mater. Sci. Forum*, 2006, **516**, 470.
11 C. D. Nunes, J. Pires, A. P. Carvalho, M. J. Calhorda and P. Ferreira, *Microporous Mesoporous Mater.*, 2008, **111**, 612.
12 Y. Ide, Y. Iwasaki and M. Ogawa, *Langmuir*, 2011, **27**, 2522.
13 M. Ogawa, M. Miyoshi and K. Kuroda, *Chem. Mater.*, 1998, **10**, 3787.
14 M. Ogawa, S. Okutomo and K. Kuroda, *J. Am. Chem. Soc.*, 1998, **120**, 7361.
15 I. Fujita, K. Kuroda and M. Ogawa, *Chem. Mater.*, 2005, **17**, 3717.
16 J. Pires, M. Pinto, J. Estella and J. C. Echevería, *J. Colloid Interface Sci.*, 2008, **317**, 206.
17 G. P. Knowles, J. V. Graham, S. W. Delaney and A. L. Chaffee, *Fuel Process. Technol.*, 2005, **86**, 1435.
18 P. J. E. Harlick and A. Sayari, *Ind. Eng. Chem. Res.*, 2006, **45**, 3248.
19 C. Knofel, J. Descarpentries, A. Benzaouia, V. Zelenak, S. Mornet, P. L. Llewellyn and V. Hornebecq, *Microporous Mesoporous Mater.*, 2007, **99**, 79.

20 H. M. Moura, F. A. Bonk, R. C. G. Vinhas, R. Landers and H. O. Pastore, *CrystEngComm*, 2011, **13**, 5428.
21 H. Y. Zhu, Z. Ding, C. Q. Lu and G. Q. Lu, *Appl. Clay Sci.*, 2002, **20**, 165.
22 S. F. Wang, M. L. Lin, Y. N. Shieh, Y. R. Wang and S. J. Wang, *Ceram. Int.*, 2007, **33**, 681.
23 S. B. Johnson, C. J. Drummond, J. P. J. Scales and S. Nishimura, *Langmuir*, 1995, **11**, 2367.
24 Y. Huang, Z. Jiang and W. Schwieger, *Chem. Mater.*, 1999, **11**, 1210.
25 K. Isoda, K. Kuroda and M. Ogawa, *Chem. Mater.*, 2000, **12**, 1702.
26 R. B. Ferreira, C. R. Silva and H. O. Pastore, *Langmuir*, 2008, **24**, 14215.
27 R. M. Silverstein, F. X. Webster and D. J. Kiemle, *Spectrometric Identification of Organic Compounds*, 7th edn, John Wiley, New York, NY, 2005.
28 J. Goworek, A. Kierys, W. Gac, A. Borówka and R. Kusak, *J. Therm. Anal. Calorim.*, 2009, **2**, 375.
29 J. M. S. Silva, G. Paul, J. Bendall, C. Bisio, L. Marchese and H. O. Pastore, *Phys. Chem. Chem. Phys.*, 2013, **15**, 13434–13445.
30 G. B. Superti, E. C. Oliveira, H. O. Pastore, G. Gatti and L. Marchese, *Chem. Mater.*, 2007, **19**, 4300.
31 J. Pires and M. L. Pinto, Pillared Interlayered Clays as Adsorbents of Gases and Vapors, in *Pillared Clays and Related Catalysts*, ed. A. Gil, *et al.*, 2010.
32 F. Kooli, *Microporous Mesoporous Mater.*, 2014, **184**, 184.
33 L. J. Michot and T. J. Pinnavaia, *Chem. Mater.*, 1992, **4**, 1433.
34 G. Fetter, D. Tichit, P. Massiani, R. Dutartre and F. Figueras, *Clays Clay Miner.*, 1994, **42**, 161.
35 P. W. J. G. Wijnen, J. W. H. Beelen, C. P. J. Rummens, L. J. M. van de Ven and R. A. Santen, *J. Non-Cryst. Solids*, 1989, **109**, 85.
36 Z. Luan, J. A. Fournier, J. B. Wooten and D. E. Miser, *Microporous Mesoporous Mater.*, 2005, **83**, 150.
37 A. Danon, P. C. Stair and E. Weitz, *J. Phys. Chem. C*, 2011, **115**, 11540.
38 K. O. Moura and H. O. Pastore, *Environ. Sci. Technol.*, 2013, **47**, 12201.
39 K. Bhattacharyya, A. Danon, B. K. Vijayan, K. A. Gray, P. C. Stair and E. Weitz, *J. Phys. Chem. C*, 2013, **117**, 12661.